ANNUAL REVIEWS

Annual Review of Biophysics

Bacterial Electrophysiology

Wei-Chang Lo,[1] Ekaterina Krasnopeeva,[2] and Teuta Pilizota[3]

[1]Institute of Physics, Academia Sinica, Taipei, Taiwan

[2]Institute of Science and Technology Austria, Klosterneuburg, Austria

[3]School of Biological Sciences, Centre for Engineering Biology, University of Edinburgh, Edinburgh, United Kingdom; email: teuta.pilizota@ed.ac.uk

Annu. Rev. Biophys. 2024. 53:487–510

First published as a Review in Advance on February 21, 2024

The *Annual Review of Biophysics* is online at biophys.annualreviews.org

https://doi.org/10.1146/annurev-biophys-030822-032215

Keywords

bacteria, electrophysiology, ion fluxes, biophysical models, pump-leak equations, membrane potential

Abstract

Bacterial ion fluxes are involved in the generation of energy, transport, and motility. As such, bacterial electrophysiology is fundamentally important for the bacterial life cycle, but it is often neglected and consequently, by and large, not understood. Arguably, the two main reasons for this are the complexity of measuring relevant variables in small cells with a cell envelope that contains the cell wall and the fact that, in a unicellular organism, relevant variables become intertwined in a nontrivial manner. To help give bacterial electrophysiology studies a firm footing, in this review, we go back to basics. We look first at the biophysics of bacterial membrane potential, and then at the approaches and models developed mostly for the study of neurons and eukaryotic mitochondria. We discuss their applicability to bacterial cells. Finally, we connect bacterial membrane potential with other relevant (electro)physiological variables and summarize methods that can be used to both measure and influence bacterial electrophysiology.

Contents

1. INTRODUCTION

To stay alive, bacteria, like other living cells, transduce energy. Two of the main sources of this energy are the ATP molecules and the electrochemical gradients of ions, often called ion motive forces (IMFs). In most bacteria, the IMF that serves as the main energy source is the proton motive force (PMF), while in some others, it is the sodium motive force (SMF) (118). The ATP and IMFs are the final result of bacterial metabolism, as part of either the oxidative or the substrate-level phosphorylation pathways (**Figure 1*a***). Briefly, oxidative phosphorylation utilizes the electron transport chain to export protons by oxidizing NADH, and substrate-level phosphorylation relies on ATP hydrolysis by F_1F_o-ATP synthase for the same purpose (116). ATP and IMFs are also interlinked, as either be used to make the other. Because bacteria are unicellular, their energy production is tightly linked with all the other processes in the cell. For example, the electrical potential across the membrane is generated by the charge accumulated at the membrane, which drives all ions. However, ions are also driven by their specific chemical concentration differences, where the exact concentration of ions in the cell, particularly that of protons, also matters. Lastly, bacteria maintain significant osmotic pressures (86), which depend on the difference between the extracellular and intracellular concentrations of all solutes, including ions. The result is a nontrivially intertwined set of physiological variables, which likely explains why the field of bacterial electrophysiology, despite being fundamentally important, is still nascent. Yet the bacterial cell does it: It achieves the necessary homeostasis among them all!

To understand how, in this review, we look at both the experimental and theoretical tools available to study bacterial electrophysiology. Since Luigi Galvani (55) proposed that living cells generate electricity in 1791, cardiac muscle and neuronal cells, where the electrical potential across the cellular membrane serves as a signal, have received a lot of attention. More than a century later, Hugo Fricke (49) measured the capacitance of the biological membrane, and Peter Mitchell (116) explained the PMF and its role in powering the production of ATP. The attention of scientists has since also focused on proteins involved in bioenergetics, as well as the mitochondria, the eukaryotic compartments where most energy production occurs. Consequently, the experimental tools and models available to study the electrophysiology of living cells have mostly been developed for

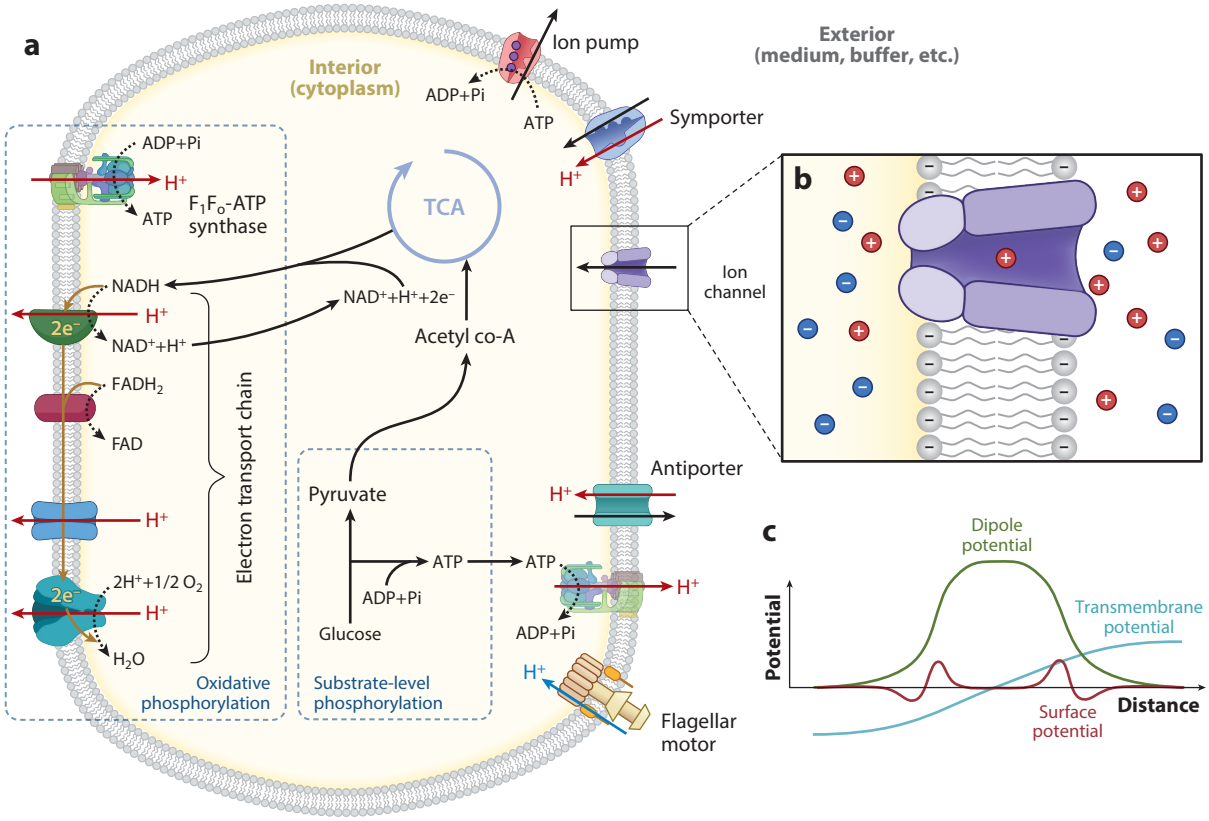

Figure 1

(*a*) A schematic diagram of a typical bacterial inner membrane and simplified energetics. The cytoplasmic membrane is shown, with common transmembrane proteins depicted (note that their number is significantly larger in the real membrane). Ion fluxes are indicated with arrows (*blue* for protons and *red* for all other ions) and coupled to bacterial metabolism. Oxidative phosphorylation utilizes the electron transport chain to export protons by oxidizing NADH. In the process, electrons are passed to oxygen, generating H_2O and regenerating NAD^+. NADH is the product of the substrate-level phosphorylation and tricarboxylic acid (TCA) cycle. The former breaks down glucose into pyruvate and ATP, and in the absence of oxidative phosphorylation, F_1F_o-ATP synthase hydrolyzes the ATP to move protons out of the cell (116). Neutrophilic bacteria now need to invest these protons, or ATP directly, to export other ions across the membrane to generate sufficient membrane potential (170). (*b*) A magnified view of the mobile monovalent cations and anions and surface charges. (*c*) A schematic diagram of the electrical potential, Ψ_m. Figure adapted from images created using BioRender.com.

neurons and cardiac cells. We therefore first discuss basic concepts relevant to bacterial electrophysiology. We then move on to discuss the tools available for modeling, measuring, and controlling it. We also include comments on approaches developed for neurons and cardiac cells, especially in light of their applicability to bacterial cells. We hope that, by the end of this review, the reader will have gained a broad understanding of major challenges that should be taken into account when studying bacterial electrophysiology and will have developed a passion for understanding it.

2. BACTERIAL MEMBRANE POTENTIAL

The key aspect of bacterial electrophysiology is the generation of membrane potential, which is enabled by a selectively permeable membrane that separates bacterial cells from the external

environment. Under physiological conditions, bacterial membranes are composed of mostly amphiphilic phospholipids that align back to back with the hydrophobic tails shielded by the hydrophilic headgroups (**Figure 1*b,c***). The bilayer organization forms a tight barrier against most polar and charged (macro)molecules (42, 57, 67, 95), although the membrane also contains a large number of proteins (3) that perform various functions and make the bilayer leaky (57, 63).

Gram-negative bacteria have two cell membranes with a peptidoglycan layer (cell wall) between them, while gram-positive bacteria have a thicker peptidoglycan layer and one inner membrane. In this section, membrane potential refers to the potential drop across the inner membrane.

The electric potential, Ψ, is a consequence of Coulomb interactions between charges and dipoles giving rise to an electrical field $\boldsymbol{E} = -\nabla\Psi$, characterized by Gauss's law:

$$\nabla \cdot \boldsymbol{E} = -\nabla^2\Psi = \frac{\rho}{\varepsilon}, \qquad 1.$$

where ρ is the distribution of charge, and ε is the permittivity.

The potential associated with the bacterial membrane, Ψ_m, can be decomposed into characteristic contributions. First, the lipid bilayer is equivalent to aligned dipoles (positive at the hydrophobic phospholipid core and negative at the surface) producing a dipole potential (**Figure 1**). Second, permanent charges located at the lipid headgroups or on the peptide chains of transmembrane proteins produce surface potential (33), which is usually significantly smaller than the dipole potential (33, 114). The most significant component of Ψ_m comes from the concentration gradient across the membrane of all ions (predominantly Na^+, K^+, and Cl^-) (135). This transmembrane potential, $\Delta\psi$, is a result of the selective permeability of the membrane and the presence of the transporter proteins that use energy (e.g., ATP) to move ions across it (**Figure 1**). $\Delta\psi$ is typically around -140 mV (negative inside the cell) (102), driving ionic flows that are indispensable for transport, energy generation, and motility (182).

Mobile ions outside of the bacterium are well-described by a Boltzmann distribution, which can be Taylor expanded in the limit of low ion concentrations and weak electrostatic potential ($|\Delta\Psi| < 25$ mV). Such a linearized Boltzman distribution, once implemented into Equation 1, leads to the Helmholtz equation $\nabla^2\Psi = \lambda^{-2}\Psi$, where λ is called the Debye length (32, 185). Solutions of the Helmholtz equation decay exponentially over the length scale λ, which is typically short (for water with 10 mM NaCl at 25°C, it is only 3 nm) but creates an inhomogeneous distribution of ionic charge close to the membrane. For a longer discussion of charge screening, the reader is referred to the extension of Section 2 in the **Supplemental Appendix**.

Supplemental Material >

Inside the cell, the environment is electroneutral, while the electric potential along the normal direction of the inner membrane decays with λ (28, 62, 114, 185). The finite size of the ions that lead to this electrical potential causes steric hindrances close to the membrane. A good model that accommodates these effects introduces a Stern layer in the vicinity of the membrane (9, 10, 125, 159), which attracts counterions to form a layer of loosely attached ions, the diffuse layer (28, 62), and together, the two form the double layer (127) (**Figure 2**). For an extended discussion on these concepts, the reader is referred to the extension of Section 2 in the **Supplemental Appendix**.

While **Figure 2** is a good model for the Ψ_m of the bacterial inner membrane, it is worth noting that the spatial distribution of charges close to the membrane that gives rise to a good model for the Ψ_m characteristic for the bacterial inner membrane has never been measured. Theoretically, the value of $\Delta\psi$ in living cells is usually estimated after a series of further approximations to the situation depicted in **Figure 2** (169), most, if not all, of which have been developed for eukaryotic cells (71). Below, we list these approximations and discuss their applicability for studies of $\Delta\psi$ in bacteria.

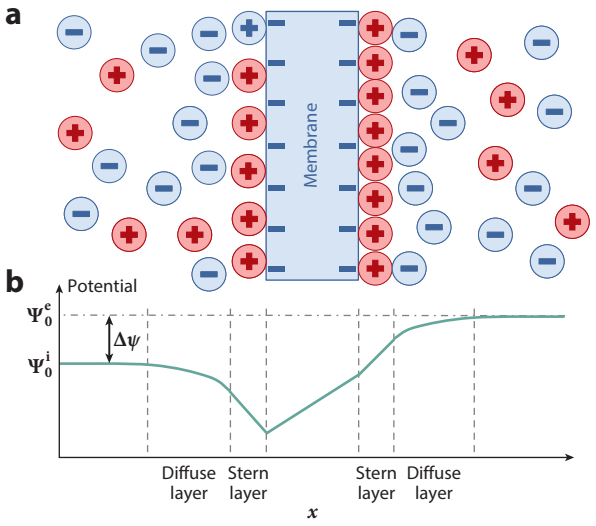

Figure 2

A schematic diagram of the double layer at an electrode–liquid interface that can be used as a good approximation for bacterial membrane and transmembrane potentials. (*a*) The ions with the opposite sign to the surface charge form the Stern layer, which attracts their counterions to form the diffuse layer. (*b*) A qualitative graphical representation of the corresponding electrical potential of the double layer, where Ψ_0^i and Ψ_0^e are the interior and exterior compartment potential, respectively.

2.1. Approximating the Transmembrane Potential

All approximations used to calculate $\Delta\psi$ consider a semipermeable, flat membrane sheet of a given thickness that separates the intracellular space from the environment (denoted by the superscripts i and e, respectively). The aqueous solution in each compartment contains various ions, each carrying an electric charge $z_j e$, where z_j is the valency of an ion j, and $[x_j]$ and x_j are its molar concentration and the number of moles, respectively. The solution is dilute, whereas the bacterial cytoplasm is very crowded (126), and hydrodynamic interactions are disregarded. The membrane is assumed to be selectively permeable to some ion species, whereas ions in the cell, like DNA, are considered impermeable. The permeable ions permeate the membrane via membrane proteins, either by leaking through them or by being transported by specific proteins. Leakage fluxes have been measured for mitochondrial membranes (57, 107). While similar fluxes are expected for bacterial membranes, these have not been characterized. All ion fluxes across the biological membrane are considered to be solely the result of the specific ion concentration gradient and $\Delta\psi$, and these vary only along the direction normal to the membrane. The separation of charges leading to $\Delta\psi$ localizes in the close vicinity of the membrane. Away from the semipermeable membrane, the intracellular environment is electrically neutral, and

$$z_{\mathrm{im}}[x_{\mathrm{im}}]^{\mathrm{i}} + \sum_j z_j[x_j]^{\mathrm{i}} = 0, \qquad 2.$$

where z_{im} is the valency of the average concentration of impermeable macromolecules, $[x_{\mathrm{im}}]$.

2.1.1. Transmembrane potential in thermodynamic equilibrium. With the approximations mentioned above, the transmembrane potential in thermodynamic equilibrium can be obtained analytically (identically for bacterial and eukaryotic cells). For this purpose, we consider the

electrochemical potential of permeable ions, as it tells us how easy it is to add an ion j at a given location in space under the influence of the electric potential:

$$\mu_j^{\mathrm{i}} = \mu_{j,0} + RT\ln([x_j]^{\mathrm{i}}) + z_j F\psi^{\mathrm{i}} \quad 3.$$

and

$$\mu_j^{\mathrm{e}} = \mu_{j,0} + RT\ln([x_j]^{\mathrm{e}}) + z_j F\psi^{\mathrm{e}}, \quad 4.$$

where $\mu_{j,0}$ is the standard chemical potential, R is the universal gas constant, T is the temperature, F is the Faraday constant, and $\psi^{\mathrm{i,e}}$ are the electric potentials (both apply to the entire compartment but, because the charge separation is localized close to the membrane, are effectively present only close to the membrane). At equilibrium, we find that $\mu_j^{\mathrm{i}} = \mu_j^{\mathrm{e}}$, and consequently

$$\Delta\psi_{j,\mathrm{eq}} = \psi_{\mathrm{eq}}^{\mathrm{i}} - \psi_{\mathrm{eq}}^{\mathrm{e}} = \frac{RT}{z_j F}\ln\left(\frac{[x_j]^{\mathrm{e}}}{[x_j]^{\mathrm{i}}}\right), \quad 5.$$

known as the Nernst potential equation, which can be understood as follows (121). Ion $[x_j]$ can permeate the membrane and so diffuses from the high- to the low-concentration side. If j is the only permeable ion, but there are $[x_{\mathrm{im}}]$ impermeable ions present in the cytoplasm, then a charge imbalance that generates an electric potential remains. The diffusion of ion $[x_j]$ is eventually balanced by this electric potential so that there is no net flux of $[x_j]$ across the membrane. The system reaches thermodynamic equilibrium, often referred to as the Gibbs-Donnan equilibrium (38, 60, 166), with $\Delta\psi$ equal to the Nernst potential.

In the cytoplasm of living cells, however, there is not just one but N permeable ions present, along with $[x_{\mathrm{im}}]$, and all these ions jointly contribute to the buildup of $\Delta\psi$. Therefore, the transmembrane potential at thermodynamic equilibrium, now called the Donnan potential (38), simultaneously equates the Nernst potential of each ion species: $\Delta\psi_{\mathrm{eq}} = \Delta\psi_{1,\mathrm{eq}} = \Delta\psi_{2,\mathrm{eq}} = \cdots = \Delta\psi_{N,\mathrm{eq}}$. Then, $[x_1]$ and $[x_2]$ need to follow the constraint

$$\left(\frac{[x_1]^{\mathrm{e}}}{[x_1]^{\mathrm{i}}}\right)^{z_2} = \left(\frac{[x_2]^{\mathrm{e}}}{[x_2]^{\mathrm{i}}}\right)^{z_1}, \quad 6.$$

and so do $[x_1]$ and $[x_3]$, $[x_2]$ and $[x_3]$, etc. A total of $\frac{1}{2}N(N-1)$ equations like Equation 6 must be satisfied in the Gibbs-Donnan equilibrium.

2.1.2. The membrane as a capacitor. Outside of thermodynamic equilibrium, cells are either in a steady state, where ion leakage and active ion transport are balanced, or in a dynamic state, characterized by nonzero net ionic fluxes. The nonequilibrium steady state corresponds to cellular homeostasis and, as such, is of particular interest. The most straightforward way to determine the nonequilibrium $\Delta\psi$ in bacteria is to take into account that, because charge separation occurs in a layer of a few nanometers next to the membrane, the membrane resembles a parallel plate capacitor. Then, each plate is assumed to be infinite and carry an equal and opposite charge per unit area σ and $-\sigma$ (**Figure 3*a***). We can obtain the electrical field between the sheets using Gauss' law in Equation 1, either by superposing two solutions for each plate or by integrating over a box (Gaussian surface) that contains both sheets. If we consider the solution for each plate, the electrical field from each is assumed to be normal to the plates and the same on each side. The Gaussian surface used to calculate $\boldsymbol{E}(x)$ for each plate is a box that cuts through the surface, and we thus obtain $E = \sigma/(2\varepsilon)$, and the superposition from both plates between them is $E = \sigma/\varepsilon = Q/(S\varepsilon)$, where Q is the total charge on each plate, and S is the plate surface area (44). The transmembrane potential in this approximation is given as

$$\Delta\psi = Q\frac{d}{S\varepsilon}, \quad 7.$$

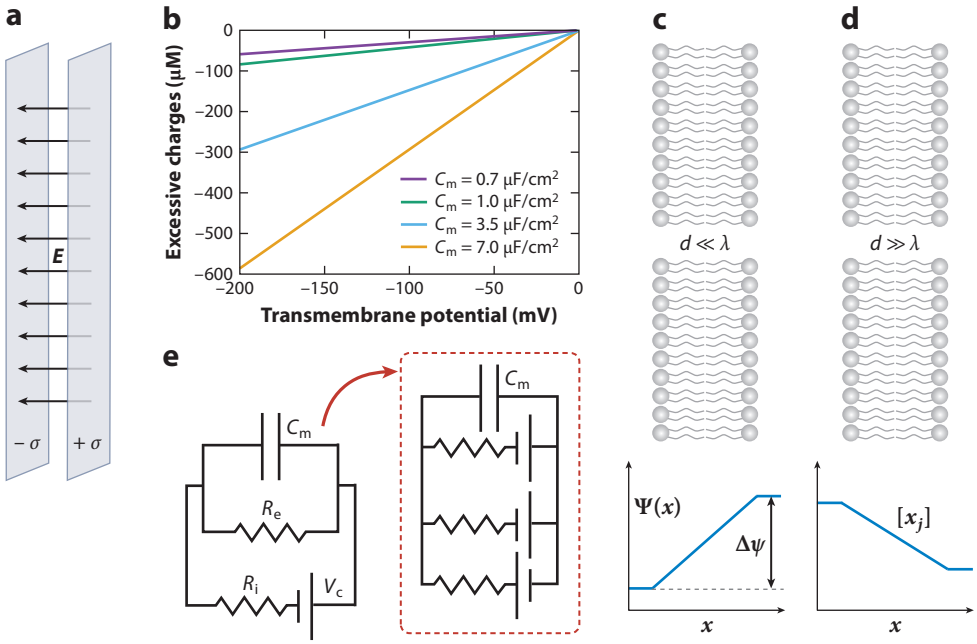

Figure 3

(*a*) The lipid bilayer can be seen as a parallel plate capacitor, with surface charge densities of σ and $-\sigma$ on each plate that generate an electric field $\boldsymbol{E}$. (*b*) The surface charge density needed to generate a given $\Delta\psi$ is calculated using Equation 8 and different C_m. (*c*) The Goldman-Hodgkin-Katz approximation is the short pore limit (the membrane sheet length, L, is much longer than its thickness, d, which is the same as the pore thickness and much shorter than the Debye length, such that $L/d \gg 1$ and $d \ll \lambda$). The electric potential inside the pore is assumed to be linear. (*d*) The chord conductance approximation is the long pore limit ($d \gg \lambda$). The concentration of monovalent salt ions is assumed to be linear within the pore. (*e*) A circuit analogy of bacterial electrophysiology.

where d is the thickness of the membrane. Given the analogy with the parallel plate capacitor, we can define the characteristic bacterial inner membrane capacitance per unit area as $C_m \equiv \sigma/\Delta\psi = \varepsilon/d$. For biological membranes, the value of C_m is approximately 1 μF/cm² (181). We can now write Equation 7 in terms of ionic concentrations and get

$$\Delta\psi(t) = \frac{FV}{C_m S}\sum_j z_j[x_j]^i(t), \qquad 8.$$

implying that C_m is constant, while $\Delta\psi$ increases or decreases with the varying capacitor surface charge. Equation 8 can be used to estimate the charge needed to generate physiologically observed $\Delta\psi$ (**Figure 3*b***). For example, at a $\Delta\psi$ of −140 mV (102) and $C_m = 1.0$ μF/cm² (181), this is equivalent to only −58.6 μM excessive charge in the cytoplasm. This is why, although it holds strictly true away from the membrane in the bulk of the cytoplasm, Equation 2 is often used as a good overall approximation.

While Equation 8 can be used to compute $\Delta\psi$ by summing the net charges on the cytoplasmic side, experimentally determining this small, spatially localized concentration of ions is not feasible in bacteria (162). Instead, experimentally estimating bacterial $\Delta\psi$ relies on a range of different approaches, which we discuss in Section 4.

2.1.3. The Goldman-Hodgkin-Katz voltage equation, ohmic conductance approach, and chord conductance equation. For eukaryotic cells, nonequilibrium steady-state $\Delta\psi$ is often obtained, both theoretically and experimentally, by solving the Nernst-Planck (NP) equation. In this section, we do so to discuss the applicability of the obtained $\Delta\psi$ equations for bacteria. The NP equation states that the flux, i.e., the amount (in moles) of ion passing through the unit area per unit of time, is proportional to the concentration gradient and the electric field:

$$J_j = -D_j\left[\nabla[x_j](\boldsymbol{x}) + \frac{z_j F}{RT}[x_j](\boldsymbol{x})\nabla\Psi(\boldsymbol{x})\right], \qquad 9.$$

where D_j is the bulk diffusion coefficient of the ion j (104, 120, 129). Equation 9 is an extension of Fick's law, with the second term describing electromigration.

One way to solve the NP equation, in addition to the approximations listed at the beginning of Section 2.1, is to assume that the membrane protein (pore) is short, the concentration of ions is low, and the electric field is constant within the pores such that $\Delta\psi$ varies linearly within it (**Figure 3*c***). Then, in the steady state and assuming that only monovalent ions are present, Equation 9 leads to the Goldman-Hodgkin-Katz (GHK) voltage equation, also known as the Goldman equation (71, 82):

$$\Delta\psi = \frac{RT}{F}\ln\left(\frac{\sum_m P_m[x_m]^{\mathrm{e}} + \sum_n P_n[x_n]^{\mathrm{i}}}{\sum_m P_m[x_m]^{\mathrm{i}} + \sum_n P_n[x_n]^{\mathrm{e}}}\right), \qquad 10.$$

where $P \equiv D_j/d$ is the specific ionic permeability (and an assumption has been made that diffusion of the ion in the pore and in the bulk is the same), and m and n sum the monovalent cations and anions, respectively.

The GHK voltage equation is a very good approximation for nerve fibers and skeletal muscles of vertebrate animals, and as such, it has been extensively used when describing the electrophysiology of these structures (24, 35, 36, 46–48). It can be generalized with divalent ions present as well (128), and it provides a way to estimate steady-state $\Delta\psi$ both computationally and experimentally. Experimentally, modulating the applied voltage in voltage clamp experiments, and various external media, enables one to estimate the permeability from the GHK approach, where the intracellular ionic concentration is usually calculated from Equation 5. For bacteria, due to their size and envelope, measuring permeability and intracellular concentrations is a difficult task (Section 4). In fact, we are not aware of measurements similar to those discussed above having been performed in bacteria. Computationally, the GHK voltage equation can still be useful for bacteria, but its applicability should be carefully considered before use.

While the GHK voltage equation assumes a constant electric field within a short pore and dilute environment, to arrive at the chord conductance equation, the pore is considered to be long, ions are allowed in the pore, and the spatial gradient of monovalent ions is a constant (**Figure 3*d***). Equation 9 can now be solved to obtain the current density for each ion, which has a form similar to that of Ohm's law (82):

$$I_j = g_j(\Delta\psi - \Delta\psi_{j,\mathrm{eq}}), \qquad 11.$$

where g_j is the conductance density of ion j in the unit of siemens per unit area. At steady state, then, we know $\sum_j I_j = 0$, which leads to the chord conductance equation (163–165),

$$\Delta\psi = \frac{g_1\Delta\psi_{1,\mathrm{eq}} + g_2\Delta\psi_{2,\mathrm{eq}} + \cdots + g_N\Delta\psi_{N,\mathrm{eq}}}{g_1 + g_2 + \cdots + g_N}. \qquad 12.$$

Equation 12 has been demonstrated to be a very good approximation for neurons of squids and frogs (73, 74, 163, 164), where voltage clamp experiments enabled direct measurements of the current–voltage relationship. It thus serves as a good way to computationally and experimentally

estimate $\Delta\psi$. In bacterial cells, again due to their size and the presence of the cell wall, patch clamping is only possible on giant spheroplasts (Section 4), and consequently, experimentally measuring g_j and intracellular concentrations is difficult. We are also not aware of any direct experimental confirmation of Equation 12's validity in bacteria, which should be kept in mind if one is using it computationally. For the derivation of Equations 10 and 12, the reader is referred to the extension of Section 2 in the **Supplemental Appendix**.

Supplemental Material >

2.2. Spatiotemporal Variations of the Transmembrane Potential

Some evidence in the literature suggests that $\Delta\psi$ in bacteria is not simply a homogeneous double layer, as depicted in **Figure 2**. For example, in *Escherichia coli*, it was suggested that F_1F_0-ATP synthase associates with bacterial flagellar motors, and that this association of proteins involved in generating or consuming cellular energy leads to higher respiratory and ATP synthesis or hydrolysis activity in their vicinity (186). Then, proton conduction at lipid–water interfaces can lead to faster proton transport compared to the bulk (2, 17, 131). It is, therefore, possible that the spatial distribution of charge separation leading to $\Delta\psi$ is not homogeneous, and that this could have physiological consequences.

Similarly, fast temporal fluctuations in $\Delta\psi$ have been reported first in *E. coli* in 2011 (89) and more recently in *E. coli*, *Bacillus subtilis*, and *Salmonella typhimurium* (78). The observations suggest the existence of fast ionic exchanges across the cell membrane, a phenomenon that was explained by a mechanism similar to that proposed by Hodgkin & Huxley (73, 74) for the firing of neuron cells, i.e., the $[Na^+]/[K^+]$ ratio in the external medium (78). Other mechanisms that might generate fluctuating $\Delta\psi$, at least in principle, include the random gating of channels (151), as well as the above-mentioned rapid transport of protons (112). Lastly, fluctuations of $\Delta\psi$ have been reported within confined bacterial communities, leading to coordinated metabolic states among cells in the interior and periphery of the biofilm (132).

3. ION FLOWS WITHIN BACTERIAL CELLS

In Section 2, we mention that bacterial cells harbor leakage and transport fluxes of ions, which are either net zero in the steady state or nonzero during dynamic transitions. Also in Section 2, we discuss how these fluxes can be described when solving NP equations under certain approximations, and in this section we wish to do so in more detail.

3.1. Pump-Leak Equations

The ion fluxes within bacterial cells can be considered explicitly via the so-called pump-leak equations (173a). Leakage of ions happens through the very large number of membrane proteins or at the membrane–protein interface (3, 57). Active transport can be ATP driven or ion electrochemical gradient driven, for instance, through ion antiporters or symporters (3). To describe how the concentration of an ion changes, we can write

$$\frac{dx_j^i}{dt} = -\frac{dx_j^e}{dt} = -S\left(J_j + \sum_p J_p\right), \qquad 13.$$

where J_j is the flux from leakage, J_p is the flux from active pumping, and S is the cell surface area.

If we assume that all individual transport and leakage reactions are reversible, and that the corresponding flux can be decomposed into the rate of import into the cell (j^+) and the rate of

export (j^-), for either a given pump or a leakage reaction, we have

$$J_{j,p} = j^+_{j,p} - j^-_{j,p} = j^+_{j,p}\left(1 - \frac{j^-_{j,p}}{j^+_{j,p}}\right), \tag{14.}$$

where $j^+_{j,p} \geq 0$ and $j^-_{j,p} \geq 0$. J_j and J_p can be further described by considering the following equation:

$$\Delta G_{j,p} \equiv \frac{RT}{F}\ln\left(\frac{j^-_{j,p}}{j^+_{j,p}}\right), \tag{15.}$$

where $\Delta G_{j,p}$ is the apparent Gibbs free energy measured in volts, which for ion j is $\Delta G_j = z_j\Delta\psi + \frac{RT}{F}\ln\frac{[x_j]^{\mathrm{i}}}{[x_j]^{\mathrm{e}}}$. For a simple chemical reaction $A + B \underset{k_-}{\overset{k_+}{\rightleftharpoons}} C + D$, it is obvious that Equation 15 holds in thermodynamic equilibrium and $\Delta G = \frac{RT}{F}\ln\left(\frac{[C][D]}{[A][B]K_{\mathrm{eq}}}\right)$, where K_{eq} is the ratio of the forward to backward rate constants, k_+ and k_-, and $j^+ = k_+[A][B]$ and $j^- = k_-[C][D]$ (13). However, Equation 15 can be generalized to open-system steady-state scenarios, including transport (12), allowing us to express the flux due to pumping or leakage as

$$J_{j,p} = j^+_{j,p}\left[1 - \exp\left(\frac{F}{RT}\Delta G_{j,p}\right)\right], \tag{16.}$$

where $j^+_{j,p}$ is a function determined by the specifics of the transport (82).

For the leakage flux of ions, j^+_j has been described by a so-called trapezoidal energy barrier model (57, 109), a general model for describing the dynamics of ionic leakage across the membrane based mostly on mitochondrial membrane data (from different cells) (57) and given as

$$j^+_j = \frac{S}{V}P^\star_j \cdot b \cdot u\frac{[x_j]^{\mathrm{e}} \cdot \mathrm{e}^{u/2} - [x_j]^{\mathrm{i}} \cdot \mathrm{e}^{-u/2}}{\mathrm{e}^{bu/2} - \mathrm{e}^{-bu/2}}, \tag{17.}$$

where $u = -\frac{F}{RT} \cdot \Delta\psi$, and b is the fractional width of the trapezoid that characterizes the shape of the voltage drop across the membrane ($0 \leq b \leq 1$) (57, 109).

The extreme values of b, 0 and 1, correspond to the Eyring (42) and the GHK flux equation, respectively. If $b = 0$, then $\Delta\psi$ within the membrane abruptly changes in the middle, such that the gradient of $\Delta\psi$ is 0 everywhere else in the membrane. Equation 16 for J_j then becomes

$$J_j = \frac{S}{V}P^\star_j \cdot [x_j]^{\mathrm{e}} \cdot \exp\left(-\frac{F}{2RT} \cdot z_j \cdot \Delta\psi\right) \cdot \left[1 - \exp\left(\frac{F \cdot \Delta G_j}{RT}\right)\right]. \tag{18.}$$

If $b = 1$, then the gradient of $\Delta\psi$ is a constant across the membrane, which we recognize as the assumption of the GHK model, and Equation 16 becomes

$$J_j = -\frac{S}{V}P^\star_j\frac{z_jF}{RT} \cdot \Delta\psi\frac{[x_j]^{\mathrm{e}}}{1 - \exp\left(\frac{z_jF}{RT}\Delta\Psi\right)} \cdot \left[1 - \exp\left(\frac{F \cdot \Delta G_j}{RT}\right)\right], \tag{19.}$$

where P_j is specific ion permeability.

Equation 19 can be obtained by solving the NP equation directly under the assumptions depicted in **Figure 3*c*** for the GHK model (13, 82) (see also the extension of Section 2 in the **Supplemental Appendix**). We now notice another assumption behind the GHK voltage equation, which is that all fluxes of ions in the given cell, not just leakage, are adequately described by Equation 19.

Supplemental Material >

For the pumping flux of ions, j^+_p is often chosen to be a constant (82, 109, 170), which implies an at least two-step reaction that always operates in the saturating regime (for all relevant input variables). For example, we have $j^+_p \approx N_p \cdot v_{\max}$, where N_p is the number of specific pumps, and

v_{max} is the maximum pump rate. In general, j_p^+ can be derived explicitly for a given pump if the specific mechanism of action either is known or can be reasonably anticipated (82).

The following descriptions of pumping and leakage have recently been used in bacterial cells (83, 144, 152). Both Schink et al. (144) and Sirec et al. (152) model the movement of ions across a cellular membrane by considering solely the chemical potential, but electrostatic forces should likely also be included. Kikuchi et al. (83) and Stratford et al. (161) use a form of the Hodgkin-Huxley pump-leak equations developed for neurons (73, 74). In this case, both J_j and J_p are described by a constant representing conductivity, multiplied by the difference between the membrane potential and Nernst potential for the given ion ($\Delta\psi - \Delta\psi_{j,eq}$). We can arrive at this approximation from Equation 16 if we assume that the system we are considering is not far from thermodynamic equilibrium. Then, the equivalent Gibbs energy is small, and we can Taylor expand the exponential of Equation 16, keeping the first term and arriving at the Hodgkin-Huxley model. The conductivity in the model is given as $g_K n^4$ for potassium, $g_{Na} m^3 h$ for sodium, and g_L for leakage, where g_K, g_{Na}, and g_L were measured experimentally for neurons, and n, m, and h are variables that describe the experimentally observed voltage-gated mechanism of neuronal sodium and potassium channels (73, 74). Thus, in applying the model to describe bacterial electrophysiology, one should ensure that the near-equilibrium requirement holds and that potassium and sodium channels in a given bacterium have similar gating properties to those found in neurons.

3.2. Coupling Ion Fluxes with Metabolism and Turgor Pressure

Ion flows due to pumping are ultimately powered by bacterial metabolism (**Figure 1*a***). The simplest way to couple the metabolic export of protons to pump-leak equations is to assume that the bacterial cell always has enough metabolic resources to actively export protons at a sufficiently high rate (170). This approach was used to propose that proton:ion antiporters have a direct role in maintaining $\Delta\psi$ in *E. coli* (170) because, at neutral pH^i and pH^e, the concentrations of protons and hydroxide ions are too low to substantially contribute to it (even if pH^i is within the 6–8 range, their contribution is, at most, ±3.5 mV). Where metabolism is limiting, one might need to consider it directly. Models of oxidative phosphorylation have been developed for eukaryotic cells (11, 87, 88, 107), but only some couple the ATP production to ion fluxes with a set of additional flux equations (11, 107). Although we are not aware of similar models for bacterial cells, the models that have already been developed are, by and large, applicable.

Lastly, ions play a role in the maintenance of bacterial osmotic (turgor) pressure, Π, which is proportional to the total solute concentration difference across the membrane (82, 86). When subjected to increases in external osmolarity, bacteria maintain their turgor pressure by accumulating osmolites, including K^+ (184). The accumulation is due to active transport powered by IMFs and ATP-driven pumps (184). As far as we are aware, models that include turgor pressure–related ion fluxes have yet to be proposed, and these will need to include cellular volume regulation. Pump-leak equations have been coupled to cell volume control for animal cells, however, under the assumption that the osmotic pressure is negligible (81). Bacterial electrophysiology is thus a unique example of nonlinearly coupled variables, each of which cells may need to keep under homeostatic control. Understanding the constraints this places on the tightness of the control is an outstanding issue.

3.3. Electrical Circuit Analogy

Building on the capacitor analogy, some headway in understanding ion fluxes can be made by representing a cell with an equivalent circuit (92, 176) (**Figure 3*e***). Kirchhoff's current laws can then be used to describe bacterial electrophysiology. In the circuit analogy, the flux of a given ion

is considered the current. All of the processes leading to $\Delta\psi$ generation, including oxidative or substrate-level phosphorylation, are considered to compose an imperfect battery with nonzero internal resistance (175). The membrane resistance (to that ion) and capacitance are connected in parallel (**Figure 3*e***). The transmembrane potential is equivalent to the drop in potential on the membrane resistance and is the only contribution to the electrochemical gradient of the ion that gives rise to the current in the circuit; i.e., the chemical gradient of the ion is zero. While all ions experience the same $\Delta\psi$, the concentration gradients of different ions can vary within bacterial cells, as can the membrane resistance to that ion. The circuit analogy can be expanded to include ion-specific currents, as shown in the inset of **Figure 3*e***. To expand the applicability of the circuit analogy to scenarios in which the chemical concentration gradient of the given ion is significant, an additional battery is included that works against $\Delta\psi$ (**Figure 3*e***, inset). The circuit now looks similar to the Hodgkin-Huxley model (74), where $\Delta\psi$ is the result of the processes in the cell, rather than being externally imposed by the patch-clamp experiment.

The circuit analogy has been recently used to discern the affected circuit component of the cell under damage and to predict its mechanism and nature (92). Similarly, it was used to understand the generation of PMF via light in *E. coli* engineered to express a light-driven proton pump from marine bacteria (17, 176).

4. METHODS USED TO MEASURE BACTERIAL ELECTROPHYSIOLOGY

Quantitative measurements of variables relevant to bacterial electrophysiology are by no means easy. Small cell size and the presence of the cell wall and, in the case of gram-negative bacteria, the outer membrane make these measurements complex and often indirect. In this section, we list a variety of methods reported in the literature and discuss their advantages, as well as their limitations.

4.1. Measuring the Transmembrane Potential

Because all ions contribute and are subjected to the transmembrane potential, it is arguably one of the most important variables to measure when studying bacterial electrophysiology. Several different approaches have been used for its quantification in live bacteria.

4.1.1. Electrodes. The most direct way to measure $\Delta\psi$ is with external electrodes, i.e., the patch-clamp experiment mentioned in Section 2. Pioneered by Hodgkin & Huxley (72) in 1939, the method has now reached the resolution of single mammalian neurons. In bacteria, it has been successfully applied only to enlarged bacterial cells stripped of the cell wall, termed giant spheroplasts (43, 76). $\Delta\psi$ can then be measured directly using microelectrodes as a voltmeter, with one electrode attached to the membrane and another grounded in the solution matching the ionic composition of the cytoplasm (**Figure 4*a***). The measurements thus obtained of $\Delta\psi$ are precise and quantitative, but because they require significant perturbations of the bacterial cell to obtain the spheroplast, they might not be representative.

4.1.2. Membrane-associated proteins and dyes. A variety of membrane-bound dyes for estimating $\Delta\psi$ were developed for use in neurons (138, 189), but only two have been used in bacteria, Di-4-ANEPPS and Di-8-ANEPPS, and both were deemed unsuitable (89, 106). The former nonspecifically adsorbed to the *B. subtilis* spore coat layer (106), while neither were able to incorporate into the *E. coli* membrane even after treatment with EDTA (89). To avoid loading issues specific to the dyes, membrane-embedded voltage-sensitive fluorescent proteins have been developed (**Figure 4*b***). Until recently, the only genetically encoded voltage probe demonstrated to

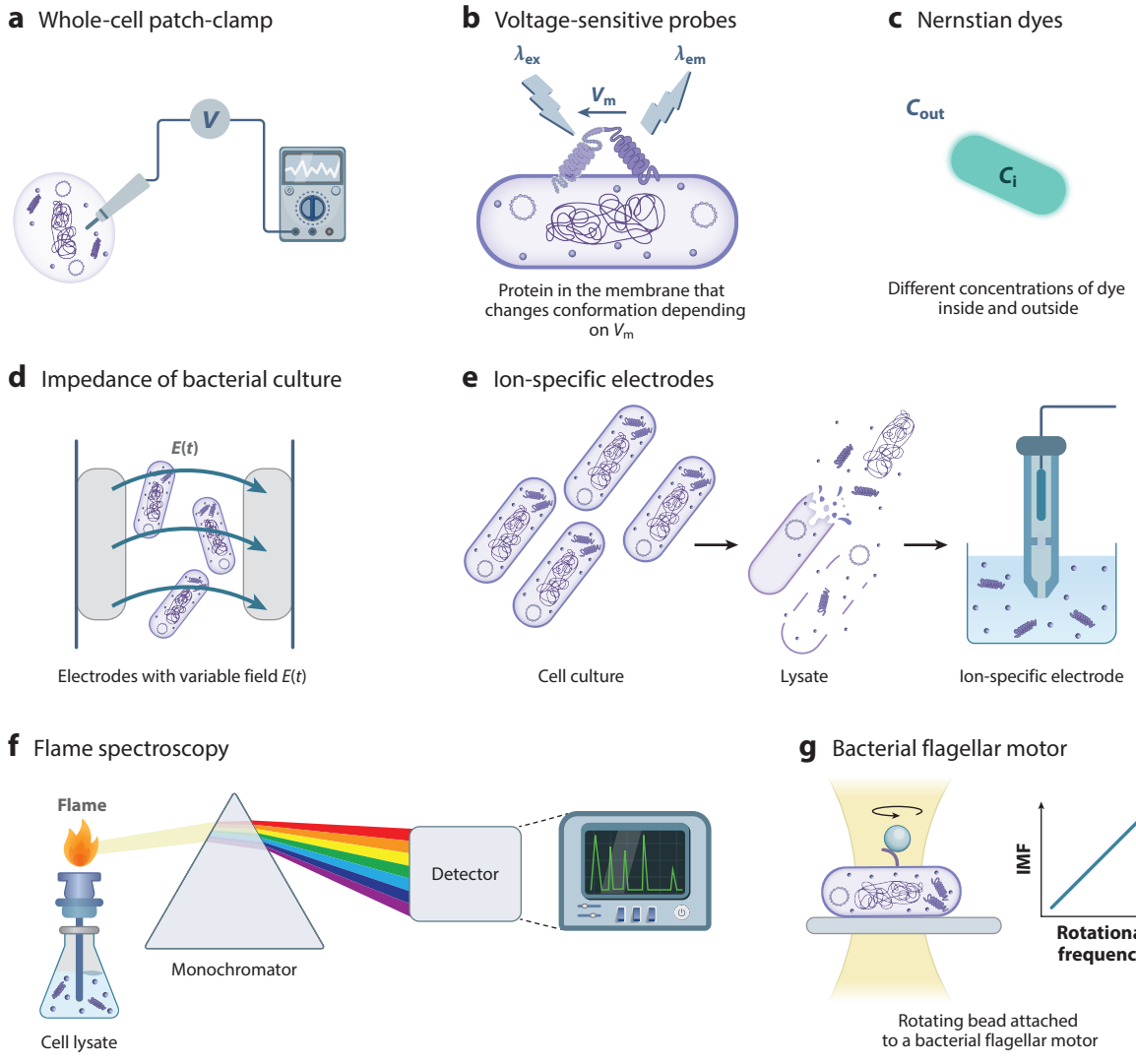

Figure 4

Schematics of some of the methods used to measure bacterial electrophysiology components. (*a*) A whole-cell patch-clamp experiment, with one electrode attached directly to the membrane of a giant spheroplast and the other grounded in an ionic solution. (*b*) A fluorescent membrane protein changing its conformation and, consequently, spectrum in response to the $\Delta\psi$ changes. (*c*) The Nernstian dye distribution across a bacterial membrane is determined by $\Delta\psi$. (*d*) The impedance of the cell culture is measured in an oscillating electric field to determine $\Delta\psi$. (*e*) Ion-selective electrodes or (*f*) flame spectroscopy are used to measure ion concentrations in the cell lysate. (*g*) The speed of a single bacterial flagella motor varies linearly with either the sodium motive force or proton motive force and can be measured with a bead assay. Abbreviation: IMF, ion motive force.

work in bacteria was proteorhodopsin optical protein sensor (PROPS), a green-absorbing proteorhodopsin (PR) engineered to act in reverse (89). Recently, ViBac1 and ViBac2 were developed and demonstrated for use in *E. coli*, *S. typhimurium*, and *B. subtilis* (78). ViBac1 was obtained by adding a bacterial membrane–targeting sequence to the N terminus of the eukaryotic transmembrane voltage sensor ArcLight, a superecliptic pHluorin derivative that is highly sensitive to the applied

voltage (with a 14-fold fluorescence increase per 100 mV) (77). ViBac2 is a fusion of ViBac1 and a voltage-inert mCherry-L protein (78), used to normalize ViBac1.

The $\Delta\psi$-dependent fluorophore spectrum changes are relative and need to be calibrated to obtain the spectrum–voltage correlation. Another consideration when using genetically encoded sensors is the potentially limited range of conditions in which the protein can be expressed. For example, PROPS is expressed at 33°C (89), and ViBac2 requires 1.5-h incubation after the removal of the inducer to allow full maturation of the proteins (78).

4.1.3. Nernstian probes. Perhaps the most commonly used method for measuring $\Delta\psi$ in bacteria is taking advantage of the Nernst equation (Equation 5). Charged fluorescent molecules, such as TMRM (102), $DiSC_3(5)$ (22, 168), $DiBac_4(3)$ (97, 108), or ThT (109, 132, 161), or radioactive molecules, such as TTP^+ (43), have been used for this purpose. The basic principle is that the (logarithm of the) chemical concentration difference of the probe molecule, quantified by measuring the fluorescence intensity or radioactive signal inside and outside of the cell, equates to $\Delta\psi$ (**Figure 4*c***). For this to hold true, the probe needs to be membrane permeable, and the whole process needs to be passive; it is not always the case that both are true. For example, ThT and $DiSC_3(5)$ can be substrates for the efflux systems of some bacteria (79, 109, 142); the permeability of the membrane could change depending on the specific conditions and the species (83, 109); and if high concentrations of the probe molecule are needed, this can substantially lower $\Delta\psi$. By definition, any concentration of the probe lowers $\Delta\psi$, and the assumption is either that the concentration used is small enough for this to be negligible or that the cell compensates for it, and that the fact that it does so does not affect the overall physiology. Thus, the suitability of charged probes for use as Nernstian $\Delta\psi$ indicators should be assessed for each condition used. The workflow for performing this assessment is summarized in Reference 109.

4.1.4. Impedance spectroscopy. Theoretical predictions suggest that the $\Delta\psi$ of the bacterial population can be estimated from the impedance measurements (59, 133, 134) (**Figure 4*d***). This method, however, is not widely used, perhaps due to its complexity.

4.2. Measuring Ion Concentrations

Apart from $\Delta\psi$, measuring $[x_j]^i$ is of interest for understanding bacterial electrophysiology, not only because the chemical potential contributes to the overall electrochemical gradient of the ion, but also because certain ions contribute to bacterial signaling (37, 84, 132), enzymatic activity (14, 64), and folding (58, 167).

4.2.1. Protons (pH). One such ion is the proton. pH homeostasis has been a subject of great interest and is probably one of the best-studied aspects of bacterial electrophysiology (103, 146, 155). The first attempts to measure the intracellular pH were made at the beginning of the twentieth century on lysed mammalian cells (23). The first reports of the internal pH of bacteria (pH^i) used dyes that change emission spectra in a pH-dependent manner. Up to 17 of such indicators were used, and surprisingly accurate results were obtained given that the process involved observing the stained bacteria under the microscope and comparing their color with the reference table by eye (66).

Currently, various quantitative probes are used. Radiolabeled membrane-permeant probes rely on the detection of the intensity or pattern of the emitted radiation, which changes depending on the probability of protonation/deprotonation (93, 188). Phosphorus-31 nuclear magnetic resonance (NMR) is based on the NMR detection of the pH-dependent chemical shifts of phosphate-containing compounds, such as phosphoric acid (H_3PO_4) or phosphate ions ($H_2PO_4^-$, HPO_4^{2-}) (1, 117). These methods, however, require high volumes of cells and, in the

case of radioactive probes, increased safety measures. The development of fluorescent probes and advances in microscopy allowed pH^i measurements to reach single-cell resolution (68, 93, 115, 149, 155). Fluorescent probes can be divided into three categories: externally added dyes, genetically encoded proteins, and the recently developed DNA-based sensors delivered into the cell by electroporation (26, 27). The variety of dyes includes primarily fluorescein-based dyes (BCECF, BCPCF, fluorescein), benzoxanthene dyes (SNAFLs, SNAFRs, SNARFs), and cyanine-based indicators (68). The main challenge in using exogenous probes is to deliver the dye into the cell cytoplasm in a concentration that is nontoxic to the cell (155). Genetically encoded probes avoid delivery problems, and while most have been designed for eukaryotic cells (85, 100, 113, 115, 140, 148, 150), pHluorins (92, 111) and cpYFP (90) have successfully been used in bacteria.

Some of the genetically encoded pH indicators change the absolute fluorescence with pH, requiring careful accounting for the number of proteins per cell and photobleaching, while others are ratiometric, i.e., excited at two different wavelengths whose emission intensity depends on the pH, for example, ratiometric pHluorin and cpYFP (115, 148). Like with the $\Delta\psi$ sensors discussed above, with all the aforementioned proton sensors, careful calibration for each condition used is necessary (178).

4.2.2. Other ions. Compared to protons, measurements of concentrations of other ions in bacteria are less common, even though they contribute significantly to $\Delta\psi$, Π, signaling, and more. The ions of particular interest to bacteria are Na^+, K^+, Ca^{2+}, and Mg^{2+}. For example, most bacteria have several Na^+-dependent membrane transporters (130, 160, 183), and as mentioned above, some use Na^+ instead of H^+ to generate ATP or power motility (69, 99, 154). K^+ is the most abundant cation in bacteria (40), and as discussed above, it plays an important role in osmoregulation (19, 39), as well as being involved in signaling within the biofilm (132). Ca^{2+} and Mg^{2+}, the two main divalent cations, serve as cofactors in many enzymatic reactions. For example, Mg^{2+} is crucial for stabilizing the membranes and ribosomes (64), and Ca^{2+} is thought to be involved in cell signaling and regulation of bacterial virulence (21, 37, 84).

The average concentration of ions within the cells can be estimated on the population level from cell lysate using ion-selective electrodes (ISEs) (**Figure 4*e***) or flame photometry (**Figure 4*f***), also known as flame emission spectroscopy (41, 162). ISEs rely on a membrane that selectively interacts with the target ion and can be used to measure H^+, Na^+, K^+, Ca^{2+}, Mg^{2+}, and Cl^- concentrations in the cell culture (162). Flame photometry is used to determine the concentration of certain elements in a sample based on their characteristic emission spectra when in a flame.

Bulk in vivo measurements of $[Na^+]^i$ were reported using ^{23}Na NMR spectroscopy (25, 119) and on single cells using Sodium Green dye, whose fluorescence increases as a function of sodium concentration (4, 101). Similarly, changes in $[K^+]^e$ in *B. subtilis* biofilms were observed with the K-specific fluorescent Asante Potassium Green-4 dye (132, 137). For $[Ca^{2+}]^i$, the ratiometric fluorescent dye fura-2 has been used in *E. coli* (56, 172), and a luminescent photoprotein aequorin, which generates blue light upon binding of the Ca^{2+} ion, has been used in *E. coli* and the cyanobacterium *Anabaena* (124, 173, 179). Free Ca^{2+} in the *E. coli* periplasm was measured by fusing aequorin with the N-terminal OmpT signal sequence to target the protein to the periplasmic space (80). Lastly, the acetoxymethyl ester form of mag-fura-2 fluorescent ratiometric dye was successfully used in *Salmonella enterica* and *B. subtilis* to report $[Mg^{2+}]^i$ (50, 180).

4.3. Measuring Electrochemical Gradients of Ions

The electrochemical potential of the relevant ion can be obtained from measurements of $\Delta\psi$ and $[x_j]^{i,e}$ with the methods discussed above. However, PMF and SMF can also be assessed directly via the bacterial flagellar motor (BFM) (**Figure 4*g***).

The BFM is one of nature's rare rotary molecular machines. It enables bacterial swimming, is the output of the bacterial chemotactic network, and is expressed over a wide range of growth conditions (30, 156). The torque generation by the BFM stator is powered by the IMF; in the case of *E. coli* or *S. typhimurium*, it is powered by the PMF, whereas in *Vibrio alginolyticus* or *Bacillus alcalophilus*, it is powered by the SMF (75). The sodium stator units derived from *V. alginolyticus* can also be expressed in *E. coli*, resulting in so-called chimeric motors (8, 157).

For the PMF-driven motors, the proportionality between the rotational speed and the PMF has been demonstrated up to at least −150 mV at both high and low loads (51, 53). Thus, measuring the changes in the BFM speed gives relative changes in the PMF (53, 91, 102, 158). In SMF-driven motors, as well as in chimeric motors, the same proportionality holds if the load on the motor is sufficiently high. However, in low-load regimes, a small nonequivalence of two components of the SMF (electrical and chemical) has been demonstrated (102, 158) and attributed to the rate-limiting Na^+ binding at low sodium concentrations and high BFM speeds. The maximum BFM torque for PMF-driven motors is 1,000–2,000 pN·nm (16, 110, 139, 156), and it is just under 4,000 pN·nm for SMF-driven motors (156, 158). It may be expected that, in high-torque regimes, the IMF–speed proportionality would saturate; however, this has not yet been observed (18). Because the BFM is a dynamic machine that changes its structure depending on the torque (98, 123, 171), and it is likely that precisely this ability allows it to hold the linear relationship between IMF and speed in a wider range of conditions (18, 91), it is possible that the saturation speed is load dependent. Thus, to use the BFM as an IMF sensor, one must consider its complex nature, e.g., to adequately choose the load on the motor, as discussed in Reference 91.

4.4. Influencing Bacterial Electrophysiology

Studies of bacterial electrophysiology can be enhanced with the ability to control its parameters in a predictable way. The generation of $\Delta\psi$ can be influenced by supplying different nutrients or limiting oxygen. For example, changing the glucose concentration in the minimal medium from approximately 1 to 100 μM doubles the PMF, while transition to the anaerobic regime can reduce it by half (147, 170). However, other bacterial physiology parameters, as well as gene expression regulation, might be altered by doing so (and the extent of change will depend on the state of bacterial cells) (145, 174). External electrodes (51, 161) or the light-powered proton pump PR (6, 171, 176) can also be used to influence $\Delta\psi$. In the first case, the external electric field will induce $\Delta\psi$ (51, 161), but this effect will not be confined to the membrane and will polarize the entire cell (7). PR will act in parallel with cell respiration to pump protons out (6, 171, 176). Blocking the generation of $\Delta\psi$ in aerobic conditions is possible with respiratory chain inhibitors, such as sodium azide, which stops cell respiration by inhibiting the activity of catalase, peroxidases, and cytochrome oxidase (53, 176).

Bacterial physiology can also be modulated by changing the membrane resistance, e.g., by the addition of various ionophores (54, 92, 176). Ionophores transport specific ions across the membrane either by shuttling them across [e.g., valinomycin (141)] or by forming an ion-specific channel [e.g., gramicidine A in gram-positive bacteria (177)], which changes the permeability of the membrane to the ion(s). Protonophores are ionophores specific to protons. The most commonly used ones include 2,4-dinitrophenol, carbonyl cyanide-*p*-trifluoromethoxyphenylhydrazone, and carbonyl cyanide *m*-chlorophenyl hydrazone. It has been demonstrated that indole (29) and butanol (92) can also act as protonophores or ionophores in *E. coli*. However, some of these protonophores and ionophores are a substrate of the bacterial efflux system as well, which can lead to markedly different responses within the population, as well as influencing the needed concentration (96). The capacitance of the bacterial membrane could be altered with temperature,

the external electric field (electrostriction) (70), or optically via membrane-bound azobenzene (31). In all cases, the change in the capacitance happens due to the change in the membrane thickness that affects the capacitor geometry. However, additional effects on cell physiology, caused by azobenzene toxicity, temperature, or electric field, must be considered.

5. CONCLUDING REMARKS

Ion fluxes play a direct role in energy generation, transport, and motility in bacteria, and are thus important enough to warrant the focus of this review. However, other electrical properties of bacteria can be relevant to their overall electrophysiology. For example, *B. subtilis* spore surface charge has been shown to be important for the spores' quality control (152), and similarly, outer surface charge could be important for antibiotic entry into the cell and, thus, treatment.

Lastly, all of the models discussed in this review assume a dilute environment, in which molecules do not interact with one another in a way that can affect their conformation. The bacterial cytoplasm, however, is very crowded (126). While this crowding is expected to affect primarily macromolecules, it is worth noting because a densely packed protein environment was observed to obstruct charge screening and enable communication between polymeric nanodipoles and retinal neurons (45).

DISCLOSURE STATEMENT

T.P. is a cofounder of the company OGI Bio Ltd., which produces microbioreactors. The other authors are not aware of any affiliations, memberships, funding, or financial holdings that might be perceived as affecting the objectivity of this review.

ACKNOWLEDGMENTS

We would like to thank all members of the Pilizota lab, as well as Calin Guet, Orkun Soyer, Munehiro Asally, Peter Swain, and in particular Matt Scott and Ariel Amir, for their support, comments, and useful discussions. T.P. and W.-C.L. were supported by the Leverhulme Trust, grant RPG-2019-187, and T.P. is supported by EPSRC Fellowship EP/V03264X/1. E.K. was supported by a European Molecular Biology Organization Long-Term Postdoctoral Fellowship, ALTF 44-2021.

LITERATURE CITED

1. Ackerman JJH, Soto GE, Spees WM, Zhu Z, Evelhoch JL. 1996. The NMR chemical shift pH measurement revisited: analysis of error and modeling of a pH dependent reference. *Magn. Reson. Med.* 36:647–83
2. Agmon N, Gutman M. 2011. Bioenergetics: proton fronts on membranes. *Nat. Chem.* 3(11):840–42
3. Alberts B, Johnson A, Lewis J, Raff M, Roberts K, Walter P. 2004. *Molecular Biology of the Cell*. New York: Garland Sci.
4. Amorino GP, Fox MH. 1995. Intracellular Na^+ measurements using sodium green tetraacetate with flow cytometry. *Cytometry* 21:248–56
5. Apell H-J. 2004. How do P-type ATPases transport ions? *Bioelectrochemistry* 63:149–56
6. Arlt J, Martinez VA, Dawson A, Pilizota T, Poon WCK. 2018. Painting with light-powered bacteria. *Nat. Commun.* 9:768
7. Arnold WM, Zimmermann U. 1982. Rotating-field-induced rotation and measurement of the membrane capacitance of single mesophyll cells of *Avena sativa*. *Z. Naturforsch.* 37:908–15
8. Asai Y, Yakushi T, Kawagishi I, Homma M. 2003. Ion-coupling determinants of Na^+-driven and H^+-driven flagellar motors. *J. Mol. Biol.* 327:453–63
9. Atkins P, De Paula J. 2006. *Atkins' Physical Chemistry*. New York: W.H. Freeman

10. Bazant MZ, Kilic MS, Storey BD, Ajdari A. 2009. Towards an understanding of induced-charge electrokinetics at large applied voltages in concentrated solutions. *Adv. Colloid Interface Sci.* 152:48–88
11. Beard DA. 2005. A biophysical model of the mitochondrial respiratory system and oxidative phosphorylation. *PLOS Comput. Biol.* 1(4):e36. Erratum. 2006. *PLOS Comput. Biol.* 2(1):e8
12. Beard DA, Qian H. 2007. Relationship between thermodynamic driving force and one-way fluxes in reversible processes. *PLOS ONE* 2(1):e144
13. Beard DA, Qian H. 2008. *Chemical Biophysics: Quantitative Analysis of Cellular Systems*. Cambridge, UK: Cambridge Univ. Press
14. Bearne SL. 2014. Illustrating the effect of pH on enzyme activity using Gibbs energy profiles. *J. Chem. Educ.* 91:84–90
15. Berg HC. 2003. The rotary motor of bacterial flagella. *Annu. Rev. Biochem.* 72:19–54
16. Berry RM, Berg HC. 1997. Absence of a barrier to backwards rotation of the bacterial flagellar motor demonstrated with optical tweezers. *PNAS* 94:14433–37
17. Biquet-Bisquert A, Carrio B, Meyer N, Fernandes TFD, Abkarian M, et al. 2023. Spatio-temporal dynamics of the proton motive force on single bacterial cells. bioRxiv 2023.04.03.535353. **https://doi.org/10.1101/2023.04.03.535353**
18. Biquet-Bisquert A, Labesse G, Pedaci F, Nord AL. 2021. The dynamic ion motive force powering the bacterial flagellar motor. *Front. Microbiol.* 12:659464
19. Booth IR, Higgins CF. 1990. Enteric bacteria and osmotic stress: intracellular potassium glutamate as a secondary signal of osmotic stress? *FEMS Microbiol. Rev.* 75:239–46
20. Bot CT, Prodan C. 2010. Quantifying the membrane potential during *E. coli* growth stages. *Biophys. Chem.* 146:133–37
21. Bruni GN, Weekley RA, Dodd BJT, Kralj JM. 2017. Voltage-gated calcium flux mediates *Escherichia coli* mechanosensation. *PNAS* 114:9445–50
22. Buttress JA, Halte M, Te Winkel JD, Erhardt M, Popp PF, Strahl H. 2022. A guide for membrane potential measurements in Gram-negative bacteria using voltage-sensitive dyes. *Microbiology* 168:001227
23. Caldwell PC. 1956. Intracellular pH. *Int. Rev. Cytol.* 5:229–77
24. Campbell DT, Hille B. 1976. Kinetic and pharmacological properties of the sodium channel of frog skeletal muscle. *J. Gen. Physiol.* 67:309–23
25. Castle AM, Macnab RM, Shulman RG. 1986. Measurement of intracellular sodium concentration and sodium transport in *Escherichia coli* by ^{23}Na nuclear magnetic resonance. *J. Biol. Chem.* 261:3288–94
26. Chakraborty S, Mizusaki H, Kenney LJ. 2015. A FRET-based DNA biosensor tracks OmpR-dependent acidification of *Salmonella* during macrophage infection. *PLOS Biol.* 13:e1002116
27. Chakraborty S, Winardhi RS, Morgan LK, Yan J, Kenney LJ. 2017. Non-canonical activation of OmpR drives acid and osmotic stress responses in single bacterial cells. *Nat. Commun.* 8:1587
28. Chapman DL. 1913. A contribution to the theory of electrocapillarity. *Lond. Edinb. Dublin Philos. Mag. J. Sci.* 25:475–81
29. Chimerel C, Field CM, Piñero-Fernandez S, Keyser UF, Summers DK. 2012. Indole prevents *Escherichia coli* cell division by modulating membrane potential. *Biochim. Biophys. Acta Biomembr.* 1818:1590–94
30. Cremer J, Honda T, Tang Y, Wong-Ng J, Vergassola M, Hwa T. 2019. Chemotaxis as a navigation strategy to boost range expansion. *Nature* 575:658–63
31. De Souza-Guerreiro TC, Bondelli G, Grobas I, Donini S, Sesti V, et al. 2023. Membrane targeted azobenzene drives optical modulation of bacterial membrane potential. *Adv. Sci.* 10:2205007
32. Debye P, Hückel E. 1923. Zur Theorie der Elektrolyte. I. Gefrierpunktserniedrigung und verwandte Erscheinungen. *Phys. Z.* 24:185–206
33. Demchenko AP, Yesylevskyy SO. 2009. Nanoscopic description of biomembrane electrostatics: results of molecular dynamics simulations and fluorescence probing. *Chem. Phys. Lipids* 160:63–84
34. Dibrova DV, Galperin MY, Koonin EV, Mulkidjanian AY. 2015. Ancient systems of sodium/potassium homeostasis as predecessors of membrane bioenergetics. *Biochemistry* 80:495–516
35. Dodge FA, Frankenhaeuser B. 1958. Membrane currents in isolated frog nerve fibre under voltage clamp conditions. *J. Physiol.* 143:76–90
36. Dodge FA, Frankenhaeuser B. 1959. Soidum currents in the myelinated nerve fibre of *Xenopus laevis* investigated with the voltage clamp technique. *J. Physiol.* 148:188–200

37. Dominguez DC. 2004. Calcium signalling in bacteria. *Mol. Microbiol.* 54:291–97
38. Donnan FG. 1911. Theorie der Membrangleichgewichte und Membranpotentiale bei Vorhandensein von nicht dialysierenden Elektrolyten. Ein Beitrag zur physikalisch-chemischen Physiologie. *Z. Elektrochem. Angew. Phys. Chem.* 17:572–81
39. Epstein W. 1986. Osmoregulation by potassium transport in *Escherichia coli*. *FEMS Microbiol. Rev.* 39:73–78
40. Epstein W. 2003. The roles and regulation of potassium in bacteria. *Prog. Nucleic Acid Res. Mol. Biol.* 75:293–320
41. Epstein W, Schultz SG. 1965. Cation transport in *Escherichia coli*. *J. Gen. Physiol.* 49:221–34
42. Eyring H, Eyring EM. 1963. *Modern Chemical Kinetics*. New York: Reinhold
43. Felle H, Porter JS, Slayman CL, Kaback HR. 1980. Quantitative measurements of membrane potential in *Escherichia coli*. *Biochemistry* 19:3585–90
44. Feynman RP, Leighton RB, Sands M. 2011. *The Feynman Lectures on Physics*. New York: Basic Books
45. Francia S, Shmal D, Di Marco S, Chiaravalli G, Maya-Vetencourt JF, et al. 2022. Light-induced charge generation in polymeric nanoparticles restores vision in advanced-stage retinitis pigmentosa rats. *Nat. Commun.* 13:3677
46. Frankenhaeuser B. 1960. Quantitative description of sodium currents in myelinated nerve fibres of *Xenopus laevis*. *J. Physiol.* 151:491–501
47. Frankenhaeuser B. 1960. Sodium permeability in toad nerve and in squid nerve. *J. Physiol.* 152:159–66
48. Frankenhaeuser B. 1963. A quantitative description of potassium currents in myelinated nerve fibres of *Xenopus laevis*. *J. Physiol.* 169:424–30
49. Fricke H. 1923. The electric capacity of cell suspension. *Phys. Rev.* 21:708–9
50. Froschauer EM, Kolisek M, Dieterich F, Schweigel M, Schweyen RJ. 2004. Fluorescence measurements of free [Mg^{2+}] by use of mag-fura 2 in *Salmonella enterica*. *FEMS Microbiol. Lett.* 237:49–55
51. Fung DC, Berg HC. 1995. Powering the flagellar motor of *Escherichia coli* with an external voltage source. *Nature* 375:809–12
52. Furst AL, Francis MB. 2019. Impedance-based detection of bacteria. *Chem. Rev.* 119:700–26
53. Gabel CV, Berg HC. 2003. The speed of the flagellar rotary motor of *Escherichia coli* varies linearly with protonmotive force. *PNAS* 100:8748–51
54. Gabrielyan L, Sargsyan H, Trchounian A. 2015. Novel properties of photofermentative biohydrogen production by purple bacteria *Rhodobacter sphaeroides*: effects of protonophores and inhibitors of responsible enzymes. *Microb. Cell Fact.* 14:131
55. Galvani L. 1791. De viribus electricitatis in motu musculari commentarius. *Bononiensi Sci. Artium Inst. Atque Acad. Comment.* 7:363–418
56. Gangola P, Rosen BP. 1987. Maintenance of intracellular calcium in *Escherichia coli*. *J. Biol. Chem.* 262:12570–74
57. Garlid KD, Beavis AD, Ratkje SK. 1989. On the nature of ion leaks in energy-transducing membranes. *Biochim. Biophys. Acta Bioenerg.* 976:109–20
58. Gasser B, Saloheimo M, Rinas U, Dragosits M, Rodríguez-Carmona E, et al. 2008. Protein folding and conformational stress in microbial cells producing recombinant proteins: a host comparative overview. *Microb. Cell Fact.* 7:11
59. Gheorghiu E. 2011. Relating membrane potential to impedance spectroscopy. *J. Electr. Bioimpedance* 2:93–97
60. Gibbs GW. 1928. *The Collected Works of J. Willard Gibbs*, Vol. I: *Thermodynamics*, ed. WR Longley, RG van Name. New York: Longmans Green Co.
61. Goldman DE. 1943. Potential, impedance, and rectification in membranes. *J. Gen. Physiol.* 27:37–60
62. Gouy LG. 1910. Sur la constitution de la charge électrique a la surface d'un électrolyte. *J. Phys. Théor. Appl.* 9:457–68
63. Grabe M, Oster G. 2001. Regulation of organelle acidity. *J. Gen. Physiol.* 117:329–44
64. Groisman EA, Hollands K, Kriner MA, Lee E-J, Park S-Y, Pontes MH. 2013. Bacterial Mg^{2+} homeostasis, transport, and virulence. *Annu. Rev. Genet.* 47:625–46
65. Guo J, Zhou H-X. 2016. Protein allostery and conformational dynamics. *Chem. Rev.* 116:6503–15

66. Gutstein M. 1933. Bestimmung der H-Konzentration in der lebenden Hefe- und Bakterienzelle. *Protoplasma* 17:454–70
67. Hall JE, Mead CA, Szabo G. 1973. A barrier model for current flow in lipid bilayer membranes. *J. Membr. Biol.* 11:75–97
68. Han J, Burgess K. 2010. Fluorescent indicators for intracellular pH. *Chem. Rev.* 110:2709–28
69. Häse CC, Fedorova ND, Galperin MY, Dibrov PA. 2001. Sodium ion cycle in bacterial pathogens: evidence from cross-genome comparisons. *Microbiol. Mol. Biol. Rev.* 65:353–70
70. Heimburg T. 2012. The capacitance and electromechanical coupling of lipid membranes close to transitions: the effect of electrostriction. *Biophys. J.* 103:918–29
71. Hille B. 2001. *Ion Channels of Excitable Membranes*. Sunderland, MA: Sinauer Assoc.
72. Hodgkin AL, Huxley AF. 1939. Action potentials recorded from inside a nerve fibre. *Nature* 144:710–11
73. Hodgkin AL, Huxley AF. 1952. Currents carried by sodium and potassium ions through the membrane of the giant axon of *Loligo*. *J. Physiol.* 116:449–72
74. Hodgkin AL, Huxley AF. 1952. A quantitative description of membrane current and its application to conduction and excitation in nerve. *J. Physiol.* 117:500–44
75. Imae Y, Atsumi T. 1989. Na^+-driven bacterial flagellar motors. *J. Bioenerg. Biomembr.* 21:705–16
76. Jiang Y, Idikuda V, Chanda B. 2021. Preparation of giant *Escherichia coli* spheroplasts for electrophysiological recordings. *Bio Protoc.* 11:e4261
77. Jin L, Han Z, Platisa J, Wooltorton JRA, Cohen LB, Pieribone VA. 2012. Single action potentials and subthreshold electrical events imaged in neurons with a fluorescent protein voltage probe. *Neuron* 75:779–85
78. Jin X, Zhang X, Ding X, Tian T, Tseng C-K, et al. 2023. Sensitive bacterial V_m sensors revealed the excitability of bacterial V_m and its role in antibiotic tolerance. *PNAS* 120:e2208348120
79. Jindal S, Yang L, Day PJ, Kell DB. 2019. Involvement of multiple influx and efflux transporters in the accumulation of cationic fluorescent dyes by *Escherichia coli*. *BMC Microbiol.* 19:195
80. Jones HE, Holland IB, Campbell AK. 2002. Direct measurement of free Ca^{2+} shows different regulation of Ca^{2+} between the periplasm and the cytosol of *Escherichia coli*. *Cell Calcium* 32:183–92
81. Kay AR. 2017. How cells can control their size by pumping ions. *Front. Cell. Dev. Biol.* 8:5–41
82. Keener JP, Sneyd J. 2009. *Mathematical Physiology*, Vol. I: *Cellular Physiology*. New York: Springer
83. Kikuchi K, Galera-Laporta L, Weatherwax C, Lam JY, Moon EC, et al. 2022. Electrochemical potential enables dormant spores to integrate environmental signals. *Science* 378:43–49
84. King MM, Kayastha BB, Franklin MJ, Patrauchan MA. 2020. Calcium regulation of bacterial virulence. *Calcium Signal.* 1131:827–55
85. Kneen M, Farinas J, Li Y, Verkman AS. 1998. Green fluorescent protein as a noninvasive intracellular pH indicator. *Biophys. J.* 74:1591–99
86. Koch A. 1985. How bacteria grow and divide in spite of internal hydrostatic pressure. *Can. J. Microbiol.* 31:1071–84
87. Korzeniewski B. 1998. Regulation of ATP supply during muscle contraction: theoretical studies. *Biochem. J.* 330:1189–95
88. Korzeniewski B. 2000. Regulation of ATP supply in mammalian skeletal muscle during resting state → intensive work transition. *Biophys. Chem.* 83:19–34
89. Kralj JM, Hochbaum DR, Douglass AD, Cohen AE. 2011. Electrical spiking in *Escherichia coli* probed with a fluorescent voltage-indicating protein. *Science* 333:345–48
90. Krasnopeeva E. 2019. *Single cell measurements of bacterial physiology traits during exposure to an external stress*. PhD Thesis, Univ. Edinburgh. **https://era.ed.ac.uk/handle/1842/35514**
91. Krasnopeeva E, Barboza-Perez UE, Rosko J, Pilizota T, Lo C-J. 2021. Bacterial flagellar motor as a multimodal biosensor. *Methods* 193:5–15
92. Krasnopeeva E, Lo C-J, Pilizota T. 2019. Single-cell bacterial electrophysiology reveals mechanisms of stress-induced damage. *Biophys. J.* 116:2390–99
93. Kurkdjian A, Guern J. 1989. Intracellular pH: measurement and importance in cell activity. *Annu. Rev. Plant Physiol. Plant Mol. Biol.* 40:271–303
94. Langosch D, Arkin IT. 2009. Interaction and conformational dynamics of membrane-spanning protein helices. *Protein Sci.* 18:1343–58

95. Läuger P, Stark G. 1970. Kinetics of carrier-mediated ion transport across lipid bilayer membranes. *Biochim. Biophys. Acta Biomembr.* 211:458–66
96. Le D, Krasnopeeva E, Sinjab F, Pilizota T, Kim M. 2021. Active efflux leads to heterogeneous dissipation of proton motive force by protonophores in bacteria. *mBio* 12:e00676-21
97. Lee W, Kim K-J, Lee DG. 2014. A novel mechanism for the antibacterial effect of silver nanoparticles on *Escherichia coli*. *BioMetals* 27:1191–201
98. Lele PP, Hosu BG, Berg HC. 2013. Dynamics of mechanosensing in the bacterial flagellar motor. *PNAS* 110:11839–44
99. Li N, Kojima S, Homma M. 2011. Sodium-driven motor of the polar flagellum in marine bacteria *Vibrio*: sodium-driven motor of the polar flagellum. *Genes Cells* 16:985–99
100. Li Y, Tsien RW. 2012. pHTomato, a red, genetically encoded indicator that enables multiplex interrogation of synaptic activity. *Nat. Neurosci.* 15:1047–53
101. Lo C-J, Leake MC, Berry RM. 2006. Fluorescence measurement of intracellular sodium concentration in single *Escherichia coli* cells. *Biophys. J.* 90:357–65
102. Lo C-J, Leake MC, Pilizota T, Berry RM. 2007. Nonequivalence of membrane voltage and ion-gradient as driving forces for the bacterial flagellar motor at low load. *Biophys. J.* 93:294–302
103. Lund PA, De Biase D, Liran O, Scheler O, Mira NP, et al. 2020. Understanding how microorganisms respond to acid pH is central to their control and successful exploitation. *Front. Microbiol.* 11:556140
104. Maex R. 2014. Nernst-Planck equation. In *Encyclopedia of Computational Neuroscience*, ed. D Jaeger, R Jung. New York: Springer. **https://doi.org/10.1007/978-1-4614-7320-6_233-1**
105. Maffeo C, Bhattacharya S, Yoo J, Wells D, Aksimentiev A. 2012. Modeling and simulation of ion channels. *Chem. Rev.* 112:6250–84
106. Magge A, Setlow B, Cowan AE, Setlow P. 2009. Analysis of dye binding by and membrane potential in spores of *Bacillus* species. *J. Appl. Microbiol.* 106:814–24
107. Magnus G, Keizer J. 1997. Minimal model of beta-cell mitochondrial Ca^{2+} handling. *Am. J. Physiol.* 273:C717–33
108. Maher MP, Wu N-T, Ao H. 2007. pH-insensitive FRET voltage dyes. *SLAS Discov.* 12:656–67
109. Mancini L, Terradot G, Tian T, Pu Y, Li Y, et al. 2020. A general workflow for characterization of Nernstian dyes and their effects on bacterial physiology. *Biophys. J.* 118:4–14
110. Mandadapu KK, Nirody JA, Berry RM, Oster G. 2015. Mechanics of torque generation in the bacterial flagellar motor. *PNAS* 112:E4381–89
111. Martinez KA, Kitko RD, Mershon JP, Adcox HE, Malek KA, et al. 2012. Cytoplasmic pH response to acid stress in individual cells of *Escherichia coli* and *Bacillus subtilis* observed by fluorescence ratio imaging microscopy. *Appl. Environ. Microbiol.* 78:3706–14
112. Marx D. 2006. Proton transfer 200 years after von Grotthuss: insights from ab initio simulations. *ChemPhysChem* 7:1848–70
113. Matlashov ME, Bogdanova YA, Ermakova GV, Mishina NM, Ermakova YG, et al. 2015. Fluorescent ratiometric pH indicator SypHer2: applications in neuroscience and regenerative biology. *Biochim. Biophys. Acta Gen. Subj.* 1850:2318–28
114. McLaughlin S. 1989. The electrostatic properties of membranes. *Annu. Rev. Biophys. Biophys. Chem.* 18:113–36
115. Miesenbock G, De Angelis DA, Rothman JE. 1998. Visualizing secretion and synaptic transmission with pH-sensitive green fluorescent proteins. *Nature* 394:192–95
116. Mitchell P. 1961. Coupling of phosphorylation to electron and hydrogen transfer by a chemi-osmotic type of mechanism. *Nature* 191:144–48
117. Moon RB, Richards JH. 1973. Determination of intracellular pH by ^{31}P magnetic resonance. *J. Biol. Chem.* 248:7276–78
118. Mulkidjanian AY, Dibrov P, Galperin MY. 2008. The past and present of sodium energetics: May the sodium-motive force be with you. *Biochim. Biophys. Acta Bioenerg.* 1777(7–8):985–92
119. Nagata S, Adachi K, Shirai K, Sano H. 1995. ^{23}Na NMR spectroscopy of free Na^+ in the halotolerant bacterium *Brevibacterium* sp. and *Escherichia coli*. *Microbiology* 141:729–36
120. Nernst W. 1888. Zur Kinetik der in Lösung befindlichen Körper. *Z. Phys. Chem.* 2:613–37

121. Nernst W. 1889. Die elektromotorische Wirksamkeit der Jonen. *Z. Phys. Chem.* 4:129–81
122. Nirody JA, Sun Y-R, Lo C-J. 2017. The biophysicist's guide to the bacterial flagellar motor. *Adv. Phys. X* 2:324–43
123. Nord AL, Gachon E, Perez-Carrasco R, Nirody JA, Barducci A, et al. 2017. Catch bond drives stator mechanosensitivity in the bacterial flagellar motor. *PNAS* 114:12952–57
124. Norris V, Grant S, Freestone P, Canvin J, Sheikh FN, et al. 1996. Calcium signalling in bacteria. *J. Bacteriol.* 178:3677–82
125. Oldham KB. 2008. A Gouy-Chapman-Stern model of the double layer at a (metal)/(ionic liquid) interface. *J. Electroanal. Chem.* 613:131–38
126. Parry BR, Surovtsev IV, Cabeen MT, O'Hern CS, Dufresne ER, Jacobs-Wagner C. 2014. The bacterial cytoplasm has glass-like properties and is fluidized by metabolic activity. *Cell* 156(1–2):183–94
127. Petsev DN, Van Swol F, Frink LJD. 2021. *Molecular Theory of Electric Double Layers*. Bristol, UK: IoP Publ.
128. Pickard WF. 1976. Generalizations of the Goldman-Hodgkin-Katz equation. *Math. Biosci.* 30:99–111
129. Planck M. 1890. Über die Erregung von Elektricität und Wärme in Elektrolyten. *Wied. Ann. Phys.* 39:161–86
130. Poolman B, Knol J, Van Der Does C, Henderson PJF, Liang W-J, et al. 1996. Cation and sugar selectivity determinants in a novel family of transport proteins. *Mol. Microbiol.* 19:911–22
131. Prats M, Tocanne JF, Teissie J. 1987. Lateral proton conduction at a lipid/water interface. Effect of lipid nature and ionic content of the aqueous phase. *Eur. J. Biochem.* 162(2):379–85
132. Prindle A, Liu J, Asally M, Ly S, Garcia-Ojalvo J, Süel GM. 2015. Ion channels enable electrical communication in bacterial communities. *Nature* 527:59–63
133. Prodan C, Prodan E. 1999. The dielectric behaviour of living cell suspensions. *J. Phys. D* 32:335–43
134. Prodan E, Prodan C, Miller JH. 2008. The dielectric response of spherical live cells in suspension: an analytic solution. *Biophys. J.* 95:4174–82
135. Ramahi AA, Ruff RL. 2014. Membrane potential. In *Encyclopedia of the Neurological Sciences*, ed. MJ Aminoff, RB Daroff, pp. 1034–35. Amsterdam: Elsevier. 2nd ed.
136. Ramirez N, Regueiro A, Arias O, Contreras R. 2009. Electrochemical impedance spectroscopy: an effective tool for a fast microbiological diagnosis. *Biotecnol. Apl.* 26:72–78
137. Rana PS, Gibbons BA, Vereninov AA, Yurinskaya VE, Clements RJ, et al. 2019. Calibration and characterization of intracellular Asante Potassium Green probes, APG-2 and APG-4. *Anal. Biochem.* 567:8–13
138. Reeve JE, Corbett AD, Boczarow I, Kaluza W, Barford W, et al. 2013. Porphyrins for probing electrical potential across lipid bilayer membranes by second harmonic generation. *Angew. Chem. Int. Ed.* 52:9044–48
139. Reid SW, Leake MC, Chandler JH, Lo C-J, Armitage JP, Berry RM. 2006. The maximum number of torque-generating units in the flagellar motor of *Escherichia coli* is at least 11. *PNAS* 103:8066–71
140. Robey RB, Ruiz O, Santos AVP, Ma J, Kear F, et al. 1998. pH-dependent fluorescence of a heterologously expressed *Aequorea* green fluorescent protein mutant: in situ spectral characteristics and applicability to intracellular pH estimation. *Biochemistry* 37:9894–901
141. Rose L, Jenkins ATA. 2007. The effect of the ionophore valinomycin on biomimetic solid supported lipid DPPTE/EPC membranes. *Bioelectrochemistry* 70:387–93
142. Salcedo-Sora JE, Jindal S, O'Hagan S, Kell DB. 2021. A palette of fluorophores that are differentially accumulated by wild-type and mutant strains of *Escherichia coli*: surrogate ligands for profiling bacterial membrane transporters. *Microbiology* 167:001016
143. Savtchenko LP, Poo MM, Rusakov DA. 2017. Electrodiffusion phenomena in neuroscience: a neglected companion. *Nat. Rev. Neurosci.* 18:598–612
144. Schink S, Polk M, Athaide E, Mukherjee A, Ammar C, et al. 2021. Electrodiffusion phenomena in neuroscience: a neglected companion. bioRxiv 2021.11.22.469587. **https://doi.org/10.1101/2021.11.22.469587**
145. Schmidt A, Kochanowski K, Vedelaar S, Ahrné E, Volkmer B, et al. 2016. The quantitative and condition-dependent *Escherichia coli* proteome. *Nat. Biotechnol.* 34:104–10

146. Schwarz J, Schumacher K, Brameyer S, Jung K. 2022. Bacterial battle against acidity. *FEMS Microbiol. Rev.* 46:fuac037
147. Schwarz-Linek J, Arlt J, Jepson A, Dawson A, Vissers T, et al. 2016. *Escherichia coli* as a model active colloid: a practical introduction. *Colloids Surf. B* 137:2–16
148. Schwarzlander M, Wagner S, Ermakova YG, Belousov VV, Radi R, et al. 2014. The "mitoflash" probe cpYFP does not respond to superoxide. *Nature* 514:E12–14
149. Schwiening C. 1999. Measurement of intracellular pH: a comparison between ion-sensitive microelectrodes and fluorescent dyes. In *Regulation of Tissue pH in Plants and Animals: A Reappraisal of Current Techniques*, ed. S Egginton, EW Taylor, JA Raven, pp. 1–18. Cambridge, UK: Cambridge Univ. Press
150. Shaner NC, Campbell RE, Steinbach PA, Giepmans BNG, Palmer AE, Tsien RY. 2004. Improved monomeric red, orange and yellow fluorescent proteins derived from *Discosoma* sp. red fluorescent protein. *Nat. Biotechnol.* 22:1567–72
151. Sigworth FJ. 1980. The variance of sodium current fluctuations at the node of Ranvier. *J. Physiol.* 307:97–129
152. Sirec T, Benarroch JM, Buffard P, Garcia-Ojalvo J, Asally M. 2019. Electrical polarization enables integrative quality control during bacterial differentiation into spores. *iScience* 16:378–89
153. Skulachev VP. 1978. Membrane-linked energy buffering as the biological function of Na^+/K^+ gradient. *FEBS Lett.* 87:171–79
154. Skulachev VP. 1985. Membrane-linked energy transductions. Bioenergetic functions of sodium: H^+ is not unique as a coupling ion. *Eur. J. Biochem.* 151:199–208
155. Slonczewski JL, Fujisawa M, Dopson M, Krulwich TA. 2009. Cytoplasmic pH measurement and homeostasis in bacteria and archaea. *Adv. Microb. Physiol.* 55:1–79
156. Sowa Y, Berry RM. 2008. Bacterial flagellar motor. *Q. Rev. Biophys.* 41:103–32
157. Sowa Y, Homma M, Ishijima A, Berry RM. 2014. Hybrid-fuel bacterial flagellar motors in *Escherichia coli*. *PNAS* 111:3436–41
158. Sowa Y, Hotta H, Homma M, Ishijima A. 2003. Torque–speed relationship of the Na^+-driven flagellar motor of *Vibrio alginolyticus*. *J. Mol. Biol.* 327:1043–51
159. Stern O. 1924. Zur Theorie der elektrolytischen Doppelschicht. *Z. Elektrochem. Angew. Phys. Chem.* 30:508–16
160. Stock J, Roseman S. 1971. A sodium-dependent sugar co-transport system in bacteria. *Biochem. Biophys. Res. Commun.* 44:132–38
161. Stratford JP, Edwards CLA, Ghanshyam MJ, Malyshev D, Delise MA, et al. 2019. Electrically induced bacterial membrane-potential dynamics correspond to cellular proliferation capacity. *PNAS* 116:9552–57
162. Szatmári D, Sárkány P, Kocsis B, Nagy T, Miseta A, et al. 2020. Intracellular ion concentrations and cation-dependent remodelling of bacterial MreB assemblies. *Sci. Rep.* 10:12002
163. Takeuchi A, Takeuchi N. 1960. On the permeability of end-plate membrane during the action of transmitter. *J. Physiol.* 154:52–67
164. Takeuchi N. 1963. Effects of calcium on the conductance change of the end-plate membrane during the action of transmitter. *J. Physiol.* 167:141–55
165. Takeuchi N. 1963. Some properties of conductance changes at the end-plate membrane during the action of acetylcholine. *J. Physiol.* 167:128–40
166. Tanak Y. 2007. Membrane characteristics and transport phenomena. In *Ion Exchange Membranes: Fundamentals and Applications*, pp. 37–57. Membr. Sci. Technol. 12. Amsterdam: Elsevier
167. Tapley TL, Franzmann TM, Chakraborty S, Jakob U, Bardwell JCA. 2010. Protein refolding by pH-triggered chaperone binding and release. *PNAS* 107:1071–76
168. Te Winkel JD, Gray DA, Seistrup KH, Hamoen LW, Strahl H. 2016. Analysis of antimicrobial-triggered membrane depolarization using voltage sensitive dyes. *Front. Cell Dev. Biol.* 4:29
169. Teorell T. 1953. Transport processes and electrical phenomena in ionic membranes. *Prog. Biophys. Biophys. Chem.* 3:305–69
170. Terradot G, Krasnopeeva E, Swain PS, Pilizota T. 2021. The proton motive force determines *Escherichia coli*'s robustness to extracellular pH. bioRxiv 2021.11.19.469321. **https://doi.org/10.1101/2021.11.19.469321**

171. Tipping MJ, Delalez NJ, Lim R, Berry RM, Armitage JP. 2013. Load-dependent assembly of the bacterial flagellar motor. *mBio* 4:e00551-13
172. Tisa LS, Adler J. 1995. Cytoplasmic free-Ca^{2+} level rises with repellents and falls with attractants in *Escherichia coli* chemotaxis. *PNAS* 92:10777–81
173. Torrecilla I, Leganés F, Bonilla I, Fernández-Piñas F. 2000. Use of recombinant aequorin to study calcium homeostasis and monitor calcium transients in response to heat and cold shock in cyanobacteria. *Plant Physiol.* 123:161–76
173a. Tosteson DC, Hoffman JF. 1960. Regulation of cell volume by active cation transport in high and low potassium sheep red cells. *J. Gen. Physiol.* 44(1):169–94
174. Unden G, Becker S, Bongaerts J, Schirawski J, Six S. 1994. Oxygen regulated gene expression in facultatively anaerobic bacteria. *Antonie Van Leeuwenhoek* 66:3–22
175. van Rotterdam BJ, Crielaard W, van Stokkum IHM, Hellingwerf KJ, Westerhoff HV. 2002. Simplicity in complexity: the photosynthetic reaction center performs as a simple 0.2 V battery. *FEBS Lett.* 510:105–7
176. Walter JM, Greenfield D, Bustamante C, Liphardt J. 2007. Light-powering *Escherichia coli* with proteorhodopsin. *PNAS* 104:2408–12
177. Wang F, Qin L, Pace CP, Wong P, Malonis R, Gao J. 2012. Solubilized gramicidin A as potential systemic antibiotics. *ChemBioChem* 13:51–55
178. Wang Y, Krasnopeeva E, Lin S, Bai F, Pilizota T, Lo C. 2019. Comparison of *Escherichia coli* surface attachment methods for single-cell microscopy. *Sci. Rep.* 9:19418
179. Watkins NJ, Knight MR, Trewavas AJ, Campbell AK. 1995. Free calcium transients in chemotactic and non-chemotactic strains of *Escherichia coli* determined by using recombinant aequorin. *Biochem. J.* 306:865–69
180. Wendel BM, Pi H, Krüger L, Herzberg C, Stülke J, Helmann JD. 2022. A central role for magnesium homeostasis during adaptation to osmotic stress. *mBio* 13:e00092-22
181. White SH. 1970. A study of lipid bilayer membrane stability using precise measurements of specific capacitance. *Biophys. J.* 10:1127–48
182. Williams JA. 1970. Origin of transmembrane potentials in non-excitable cells. *J. Theor. Biol.* 28:287–96
183. Wilson TH, Ding PZ. 2001. Sodium-substrate cotransport in bacteria. *Biochim. Biophys. Acta Bioenerg.* 1505:121–30
184. Wood JM. 2007. Bacterial osmosensing transporters. *Methods Enzymol.* 428:77–107
185. Wright MR. 2007. *An Introduction to Aqueous Electrolyte Solutions*. Hoboken, NJ: Wiley
186. Zarbiv G, Li H, Wolf A, Cecchini G, Caplan SR, et al. 2012. Energy complexes are apparently associated with the switch-motor complex of bacterial flagella. *J. Mol. Biol.* 416(2):192–207
187. Zhang F, Wang S, Yang Y, Jiang J, Tao N. 2021. Imaging single bacterial cells with electro-optical impedance microscopy. *ACS Sens.* 6:348–54
188. Zilberstein D, Agmon V, Schuldiner S, Padan E. 1984. *Escherichia coli* intracellular pH, membrane potential, and cell growth. *J. Bacteriol.* 158:246–52
189. Zochowski M, Wachowiak M, Falk CX, Cohen LB, Lam YW, et al. 2000. Imaging membrane potential with voltage-sensitive dyes. *Biol. Bull.* 198:1–21